



## Article

# Tilt-to-Length Coupling Analysis of an Off-Axis Optical Bench Design for NGGM

Kailan Wu <sup>1,2</sup>, Jingui Wu <sup>2</sup>, Bo Peng <sup>2,3</sup>, Jianjun Jia <sup>4</sup>, Honggang Luo <sup>1</sup>, Yun Wang <sup>2</sup>, Yongchao Zheng <sup>2</sup>, Yichao Yang <sup>4,\*</sup> , Xuling Lin <sup>2</sup> and Yun-Kau Lau <sup>1,3</sup>

<sup>1</sup> School of Physical Science and Technology, Lanzhou University, Lanzhou 730000, China; wukl2021@lzu.edu.cn (K.W.); luohg@lzu.edu.cn (H.L.); lau@amss.ac.cn (Y.-K.L.)

<sup>2</sup> Beijing Institute of Space Mechanics and Electricity, China Academy of Space Technology, Beijing 100094, China; wujg16@lzu.edu.cn (J.W.); peinberg@amss.ac.cn (B.P.); wangyun1104@hotmail.com (Y.W.); laser0371@163.com (Y.Z.); gezila@sina.cn (X.L.)

<sup>3</sup> Morningside Center of Mathematics, Chinese Academy of Sciences, Beijing 100190, China

<sup>4</sup> Shanghai Institute of Technical Physics, Chinese Academy of Sciences, Shanghai 200083, China; jjjun10@mail.sitp.ac.cn

\* Correspondence: yangyichao@mail.sitp.ac.cn

**Abstract:** A new off-axis optical design alternative to that of the GRACE Follow-on mission for future NGGM missions is considered. In place of the triple-mirror assembly of the GRACE Follow-on mission, a laser retro-reflector is instead generated by means of lens systems. The receiving (RX) beam and transmitting (TX) beam are enforced to be anti-parallel by a control loop with differential wavefront sensing (DWS) signals as readout, and a fast-steering mirror is employed to actuate the pointing of the local beam. The tilt-to-length (TTL) coupling noise of the new off-axis optical bench layout is carefully studied in the present work. Local TTL originated from piston noise as well as assembly and alignment errors of optical components are studied. Effort is also made to have an in depth understanding of global TTL due to relative attitude jitter between spacecraft. The margin of TTL noise in the position noise budget for laser ranging is examined. With an open loop control of the offset between the reference point of the optical bench and the centre of mass of a satellite, the TTL noise of the new off-axis optical bench design may be suppressed efficiently.

**Keywords:** off-axis layout; tilt-to-length coupling; NGGM



**Citation:** Wu, K.; Wu, J.; Peng, B.; Jia, J.; Luo, H.; Wang, Y.; Zheng, Y.; Yang, Y.; Lin, X.; Lau, Y.-K.

Tilt-to-Length Coupling Analysis of an Off-Axis Optical Bench Design for NGGM. *Remote Sens.* **2023**, *15*, 3915. <https://doi.org/10.3390/rs15153915>

Academic Editors: Thomas Gruber and Jean-Michel Lemoine

Received: 13 June 2023

Revised: 26 July 2023

Accepted: 28 July 2023

Published: 7 August 2023



**Copyright:** © 2023 by the authors. Licensee MDPI, Basel, Switzerland. This article is an open access article distributed under the terms and conditions of the Creative Commons Attribution (CC BY) license (<https://creativecommons.org/licenses/by/4.0/>).

## 1. Introduction

With the success of the laser ranging instrument (LRI) in the GRACE Follow-on mission, heterodyne laser interferometry is destined to become a preferred ranging method to measure the miniature range variation between two satellites and map the earth gravity field for future NGGM missions [1]. With the MAGIC mission by NASA/ESA planned to launch a Bender pair of satellites around 2030 [2], satellite gravity will enter a new era of development. The recent success of the first satellite-to-satellite tracking mission in China has also prompted ongoing discussions and debates on what the second generation of gravity missions would be like for China [3]. While the optical design for future MAGIC missions is likely to be based on the heritage of the off-axis triple-mirror assembly (TMA) demonstrated in the GRACE Follow-on mission [4], the mission architecture, and optical design in particular, for future prospective NGGM missions for China is still open. As far as optical design is concerned, an off-axis design is preferred as it minimises the coupling of attitude jitter to the optical path length. However, it is preferable to integrate the function of TMA into the optical bench [5], in contrast to the separation of the optical bench and the TMA in current GFO design. In doing so, we hope to have a more compact and light-weight optical bench. Further, when we look to the long-term future in satellite gravity development, in order to overcome the current outstanding AOD aliasing problem

generated by the high frequency mass variation signals due to atmosphere and ocean tides, more pairs of satellites are required to enhance the temporal resolution of gravity signals. The desire to realise this multi-pairs scenario and yet keep the financial budget of the mission to a reasonable level naturally leads us to look at the miniaturization of satellites with light-weight payloads (see [6]). Gravity signals with a high sampling rate in time also means that we may turn the atmospheric forcing and ocean tides into signals instead of noises so that the scientific scope of satellite gravity may be broadened.

As a modest first step to explore the feasibility of the miniaturization of satellites for satellite gravity, we are currently looking at the option of adopting a more compact optical design for future prospective NKGGM missions for China. A new mission architecture is currently under study [7], in which, in place of the triple-mirror assembly adopted in the GRACE Follow-on mission, an optical system comprising lens and rooftop mirrors is employed to generate laser retro-reflection between two satellites. The receiving (RX) beam and transmitting (TX) beam are enforced to be anti-parallel by a control loop with the differential wavefront sensing signal readout from the quadrant photodiodes (QPD) as the controller, and a fast-steering mirror is employed to actuate the pointing of the local beam. An open loop is also designed so that we have the flexibility to adjust on orbit the distance variation between the centre of mass of a satellite and the phase centre of the optical design. This will enable us to minimise the tilt-to-length (TTL) coupling noise in the laser metrology system, which will lead to improvement in the laser ranging accuracy, without the need to subtract the phase centre offset in the post data processing. Due to the presence of the AOD noise in the gravity field recovery, currently the enhancement in sensitivity in the laser ranging will not improve the precision in the measurement of the temporal variation of the gravity field. Still, the precision of static gravity field recovery will benefit, and it is conceivable that, in the long term, when we have more pairs of satellites to improve the temporal resolution of gravity signals, enhancement in the laser ranging precision will help improve the precision in the measurement of the temporal variation of gravity.

In a previous work [7], the viability of the new optical design was demonstrated in a preliminary way. However, the assembly and alignment errors of the optical components are not considered and a certain idealistic assumption is also made on the coincidence of the phase centre of the optical system with the centre of mass of a satellite. As a result, the TTL coupling noise is grossly underestimated. It is the aim of the present work to consider a more realistic scenario and strive to understand in depth, both the local as well as the global TTL coupling noise. This will pave the way for their possible mitigation in the prototype development stage.

The paper is structured as follows. In Section 2, the detailed design of the off-axis optical bench layout is presented, with more refinements added compared with the previous design. Section 3 presents the analysis of the local TTL originated from the assembly and alignment errors of optical components. With the employment of 1B data on star sensors from the GFO mission, in Section 4 we probe into the global TTL noise generated by the relative attitude jitter between two spacecraft. Some remarks are made concerning future work in Section 5 to conclude the present work.

## 2. Off-Axis Optical Bench Design

To make the present work self contained, we shall first give a brief description of the new proposed off-axis optical bench layout [7]. We shall also add a few refined details to the optical design.

Compared with the optical design of the Grace Follow-on mission, our proposed off-axis optical bench layout is more compact in that there is no separation of the triple-mirror assembly with the optical bench. Instead, a combination of lens systems and rooftop mirrors is employed to generate a laser retro-reflector. Lens systems are also used to image the rotation of the beams to the centre of the photodiodes and the transmitter reference point. Further, an open loop control is added to minimise on orbit the offset between the

phase centre and the centre of mass of a satellite. As we shall see in a moment, the TTL coupling of the proposed off-axis optical bench may be efficiently suppressed.

The design of the off-axis optical bench is shown in Figure 1. Clipped by the receiving aperture, the receiving (RX) beam emitted by the remote satellite transmits through lens L1 and is then split by beamsplitter BS1. Approximately 90% of the initial RX beam is equally split by beamsplitter BS2, then passes through lenses L4 and L5, respectively, and is then captured by the quadrant photodiodes. The local (LO) Gaussian beam enters the optical bench through a fibre coupler, and the waist of the beam is placed at the surface of the fast-steering mirror (FSM). After passing through lens L2 and being split by BS1, 10% of the initial LO beam is reflected to BS2 and then interferes with the RX beam, while the majority of the split beam transmits to lens L3 and is then reflected by the rooftop mirrors M1 and M2; it then propagates to the remote satellite. The angle between the rooftop mirrors is set to be  $135^\circ$ , and both mirrors are perpendicular to the baseplate. In addition, both beamsplitters employed in the optical bench have a wedge of  $0.5^\circ$ , which serve to reduce the impact of the back scattered stray light. The reference point of the optical setup is denoted by RP.

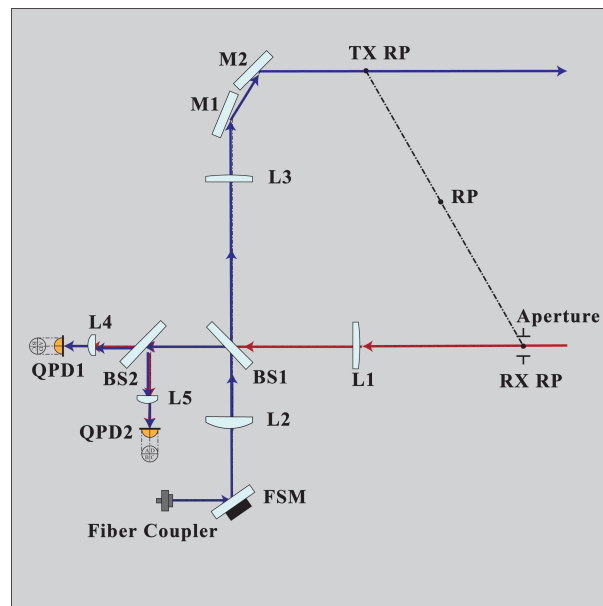


**Figure 1.** Schematic drawing of the off-axis optical bench design. The RX beam and TX beam enter and exit the optical bench through different light paths.

The interfering beams are received by the quadrant photodiodes QPD1 and QPD2. The phase signals derived from the beatnotes are then used to calculate the longitudinal pathlength signal (LPS) variations and the differential wavefront sensing signals. An automatic beam alignment system based on the DWS signals is employed in the optical bench in order to compensate the misalignment caused by the attitude jitter of the satellites [8]. The angular motion of the satellites results in an additional tilt of the RX beam when it impinges on the QPDs. The horizontal and vertical DWS signals are then used to measure the relative angle between the interfering beams, which will be fed back to the FSM mirror. In this way, the LO beam is steered by the FSM, yielding a zero value in the  $DWS_h$  and  $DWS_v$  and forcing the interfering beams to be parallel again [8,9]. We shall call this process DWS feedback control.

Five keplerian telescope lens systems are employed in this optical layout: L1-L4 and L1-L5 as the RX lens systems; L2-L4 and L2-L5 as the LO lens systems; and L2-L3 as the TX lens systems. The points of rotation of the beams are imagined to the centre of the photodiodes by the lens systems, and the optical path lengths between the front and back focal points of the lens systems are supposed to be unchanged; thus, the beam walk is

minimized. In addition, the beams are expanded and compressed through the lens systems, so that the sizes of the beams are adjusted to match the active area of the QPDs [9]. The front focus of L1 is placed at the centre of the receiving aperture, while the back focal points of L4 and L5 locate at the centre of the active area of the QPDs. The front focal point of L2 is put on the surface of the FSM, and the back focus of L3 is placed at the transmitter reference point (TX RP). The receiver reference point (RX RP) locates at the centre of the receiving aperture, and the centre of the RX RP and TX RP is designated as the reference point (RP) of the optical bench, which is supposed to coincide with the centre of mass (CoM) of the spacecraft, as well as the accelerometer reference point [8]. The relationship of the angular magnifications among these three lens systems is supposed to be [9]:

$$|m_{a,rx}| = \frac{|m_{a,lo}|}{|m_{a,tx}|}. \quad (1)$$

where  $m_{a,rx}$ ,  $m_{a,lo}$ ,  $m_{a,tx}$  denote, respectively, the angular magnifications of the RX, LO, and TX lens systems. The RX and TX beams are maintained to be anti-parallel in the off-axis setup with a combination of lens systems and mirrors, under the control of the DWS feedback loop.

Not all optical components are equal in terms of their impacts on the optical pathlength difference (OPD); some are more equal than others. We divide the optical components into critical and uncritical categories. For the off-axis layout, beamsplitter BS1, the rooftop mirrors, and lenses L1, L2, and L3 are critical components, which should be carefully aligned. Those critical components work as beam combiners as well as components directing the beam to a readout target, whose misalignments will cause a significant variation in OPD [10]. The alignment of lenses L4 and L5 are less stringent due to a common mode cancellation of the OPD changes of the incident beams. The effect of the misalignment of the FSM is significant on the local optical bench but can be mostly eliminated when considering the global situation. Beamsplitter BS2 may be categorized as a non-critical component which serves only to split the interfering beams and has a negligible impact on the OPD.

Our former work gives a preliminary investigation of the off-axis optical bench by considering a smaller waist radius of 1 mm for the LO beam. To achieve the higher heterodyne efficiency and carrier-to-noise ratio (CNR), the waist radius of the LO beam is enlarged to 2.5 mm, in line with that of the GRACE Follow-on mission, and the parameters of the lenses are chosen to be identical to those of an on-axis optical bench design [9]. The parameters adopted in the simulation are based on the commercial components shown in Table 1. The RX beam clipped by the receiving aperture has an approximately flat wavefront and a constant intensity behind the aperture, known as a flat-top beam [8,11]. A mode expansion method (MEM) is applied to simulate the propagation of a flat-top beam within the optical bench [9,11].

**Table 1.** Parameters of the optical components used in the simulation:  $r_{RX,AP}$  is the radius of the receiving aperture;  $\omega_0$  is the waist radius of the LO beam;  $\eta$  is the calculated heterodyne efficiency;  $\eta_{simulated}$  is the simulated heterodyne efficiency; CNR is the carrier-to-noise ratio.

	$r_{RX,AP}$	$\omega_0$	$f_{L1,L3}$	$f_{L2}$	$f_{L4,L5}$	$ m_{a,rx}^{-1} $	$ m_{a,tx}^{-1} $	$ m_{a,lo}^{-1} $	$\eta$	$\eta_{simulated}$	CNR
Parameters	8 mm	2.5 mm	200 mm	75.6 mm	12.7 mm	0.0635	2.6455	0.1680	0.85	0.862	94.34 dB-Hz

An illustration of the simulated optical bench is given in Figure 2. All the parameters and results in the simulation are output in double precision.

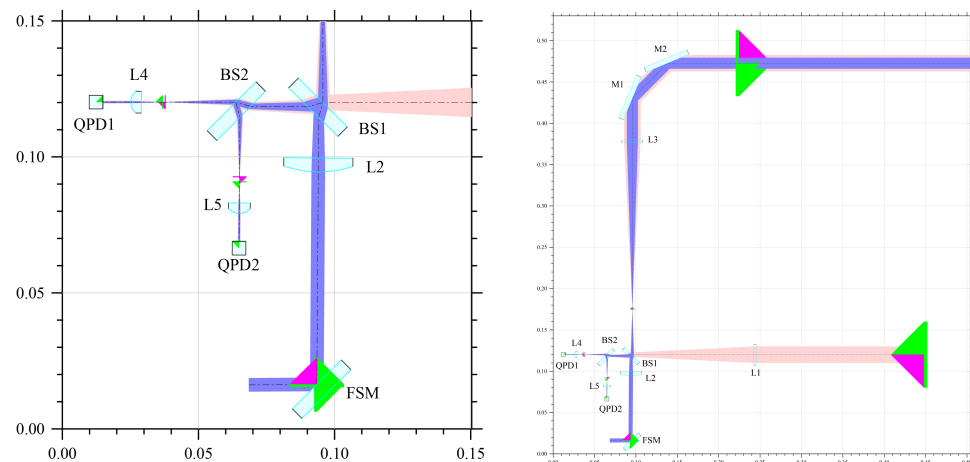


**Figure 2.** The schematic drawing of the off-axis optical bench design, output by Optocad [12]. The RX beam is in red, while the local beam and TX beam are shown in blue. The triangle markers give the position of the beam waist, the green marker is the tangential waist indicator, and the magenta marker is the sagittal waist indicators.

The initial setup of the components used in the simulation model is depicted in Figure 2. The off-axis layout is further optimized by adjusting the positions of the lenses, the QPDs, and the receiving aperture [9]. The position of lens L4 is first adjusted along the optical axis to compensate for the offset between the back focus of lens L4 and the equivalent back focus of lens L1, while the position of lens L5 is adjusted for the same purpose. Lens L3 is then adjusted to compensate for the offset between the back focus of lens L3 and the equivalent back focus of lens L2. The QPDs are fine tuned along the optical axis in order to reduce the beamwalk of the LO beam on the active areas of the photodiodes. As the last step, the receiving aperture is tuned until an optimized TTL coupling is derived, both in yaw and pitch degrees of freedom [9].

For the off-axis layout, offset exists between the reference point (RP) of the optical bench and the CoM of the satellite, which will result in a variation of OPD when coupled with the attitude jitter of the satellite. The offset may be minimised by an open loop correction mechanism. For the KBR of the GRACE or GRACE Follow-on mission, the manoeuvre is by now quite standard and is usually performed every three to six months. An accuracy of micrometers may be achieved [13]. However, when we go further up in the LRI ranging sensitivity, the limit of sensitivity for this manoeuvre is not known for the time being. This limit is not determined by the LRI ranging sensitivity alone; star sensor and the rotational degrees of freedom of the accelerometer as well as stability of the satellite platform will also play a role. After a spacecraft manoeuvre to calibrate the reference point relative to the CoM of the satellite [13], an open loop correction mechanism is activated to correct the offset on orbit. One possible design of this open loop control is to employ two FSMs to control the position of the RP point, as depicted in Figure 3. It is likely that an alternative design of this open loop control is feasible. This will be further studied in future work.

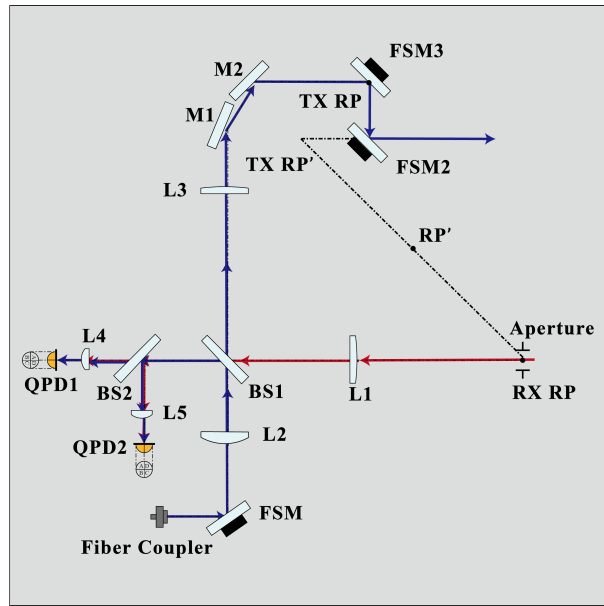


**Figure 3.** The schematic drawing of a reference point correction setup. Two more FSM mirrors (FSM2, FSM3) are added, and the position of the RP point can be corrected by steering the FSM mirrors.

### 3. Local TTL Coupling

Angular and lateral jitter of the RX beam during its propagation within the optical bench, termed local TTL coupling, will be addressed in this section. In the simulation model shown in Figure 4 [7], the RX beam is tilted in yaw and pitch degrees of freedom and LPS variation is derived, and the local TTL coupling is then calculated. For more description of TTL coupling, see [9,14].

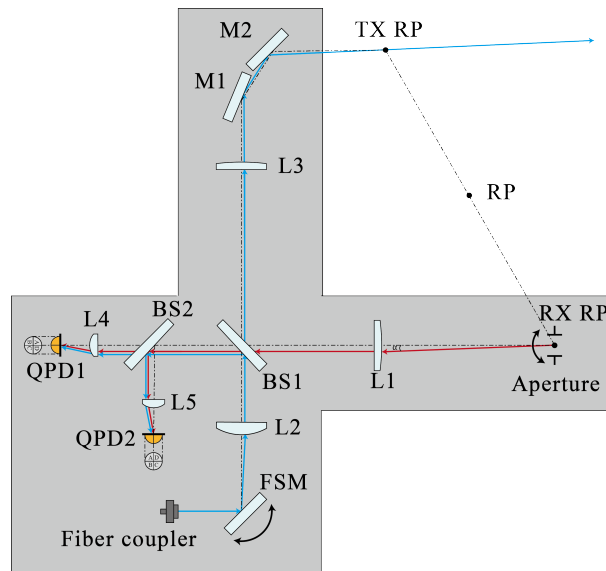


**Figure 4.** Illustration of the local TTL coupling noise in the simulation. The RX beam is rotated around the RP point in different rotational degrees of freedom [7].

To begin with, offsets due to assembly errors of the optical elements and the piston effect [14] will be considered.

### 3.1. Transmissive Optical Components

Refractive indices of optical components, the beamsplitters in particular, will generate beam walk on the surface of the photodiode detectors. To investigate the TTL coupling due to the imperfect imaging of the lens systems and the impact of the mismatch between the interfering beams, for our simulation, the beamsplitters are assumed to be made of fused silica with a refractive index of 1.458; the refractive index of mirrors and lenses is chosen to be 1.517, as in N-BK7.

The RX beam is rotated around the RX RP point for  $\pm 2$  mrad in yaw and pitch degrees of freedom, respectively. With the activation of the DWS feedback loop, the angle between the interfering beams received by the detector is minimised. LPS signals derived from the QPD1 and QPD2 are then calculated and the local TTL coupling noise is obtained. The results are shown in Figure 5. The figures depict the local TTL coupling in yaw and pitch degrees of freedom.

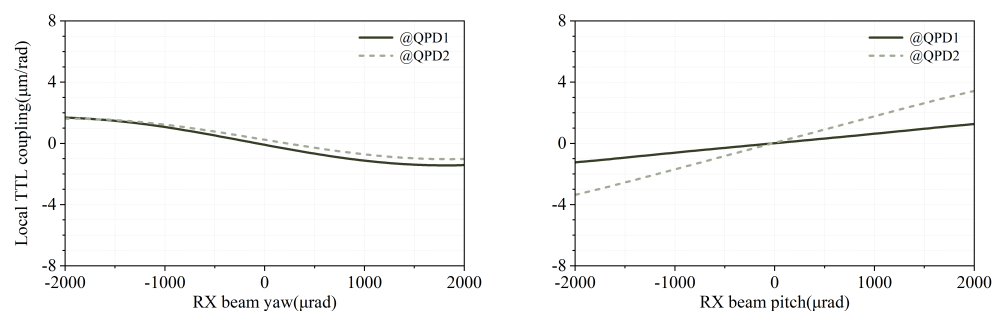


**Figure 5.** Results of the local TTL coupling simulation. The figures depict the local TTL coupling in yaw and pitch degrees of freedom.

### 3.2. Piston Effect

For the off-axis layout, imaging systems are employed to minimize the beamwalk on the photodiodes, and with this setup the lever arm effect is significantly suppressed. We will only consider the piston effect in what follows. Depicted in Figure 6, piston noise is generated due to the offset between the geometric centre and the pivotal point of the FSM [14].

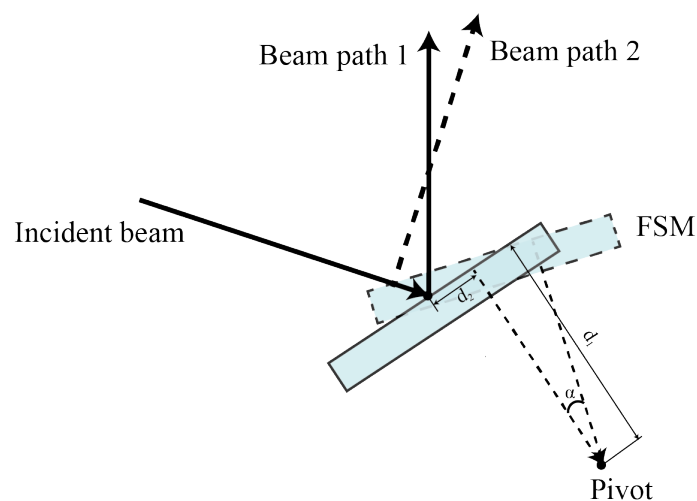


**Figure 6.** Illustration of the piston effect. The pivot of the FSM is shifted longitudinally by  $d_1$  and laterally by  $d_2$  against the reflection point. Beam path 1 represents the nominal propagation when there is no offset exists. Beam path 2, drawn in dashed lines, represents the reflective beam when the offset exists [14].

The RX beam is rotated around the RX-RP point in yaw and pitch degrees of freedom for  $\pm 2$  mrad. Local TTL coupling noise results are shown in Figure 7. For a local piston noise budget of  $3 \mu\text{m}/\text{rad}$  in both rotational degrees of freedom, the longitudinal offset between the rotation point and its nominal location should be kept under  $200 \mu\text{m}$ , while the lateral offset must be kept under  $800 \text{ nm}$ . From the experience in gravitational wave detection, the piston effect can be drastically reduced by a novel design of the FSM actuator, which minimizes the offset between the pivot and the reflection point [15].

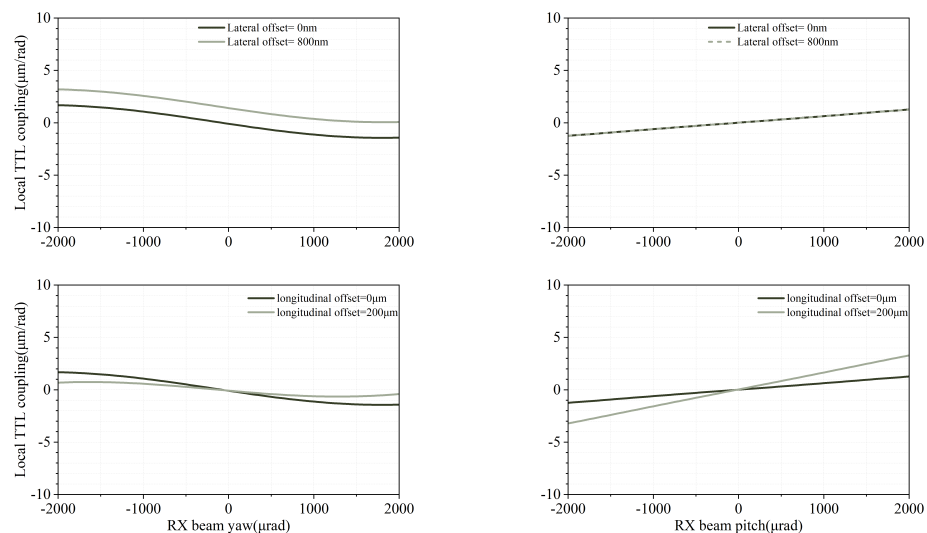


**Figure 7.** Local piston effect simulation results. The local TTL coupling variations generated by the lateral offset (**top**) and the longitudinal offset (**bottom**) are given.

### 3.3. Misalignment of the Critical Components

To evaluate the impact of misalignments of the optical components due to assembly errors, the positions of the components are slightly shifted along the  $x$ ,  $y$ , and  $z$  axes. The RX beam is then rotated around the RX RP point for  $\pm 2$  mrad in yaw and pitch degrees of freedom, and LPS signal variations derived from the QPDs are used to calculate the local TTL coupling. For the off-axis optical bench, QPD2 acts as a redundant detector, and the deployment tolerance of lens L4 is expected to be similar to lens L5, so only the LPS signal derived from the QPD1 is considered.

Depicted in Figure 8, local TTL coupling is significant in the yaw degree of freedom when L1 is misaligned on the  $y$ -axis and L2 is misaligned on the  $x$ -axis. Significant variations of local TTL coupling also exist in pitch when L1 and L2 are misaligned on the  $z$ -axis. For a positioning accuracy of  $\pm 1 \mu\text{m}$  in assembling the critical components L1 and L2, local TTL coupling variations due to the misalignment are shown in Figure 9.

### 3.4. Summary of the Local TTL Coupling

To end this section, we give a summary of the main sources of the local TTL coupling. The results are shown in Table 2. The TTL coupling coefficient is given when the RX beam rotates for 2 mrad.

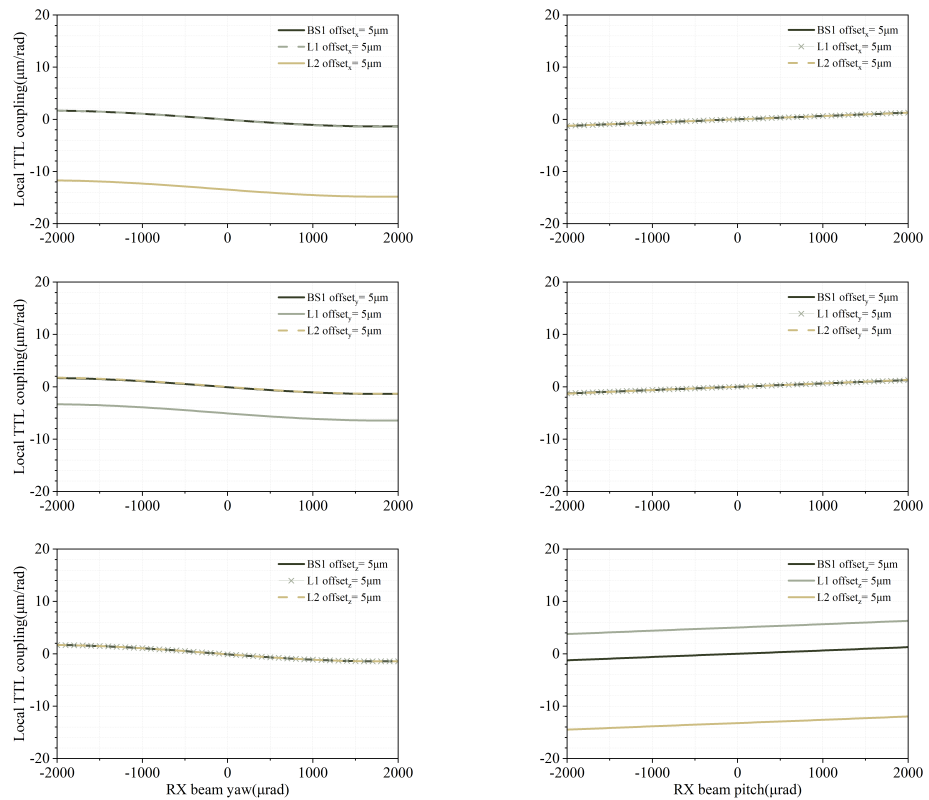


**Figure 8.** Results of the assembly errors simulation. Different offsets for the positions of the critical components along the  $x$ ,  $y$ , and  $z$  axes are considered. The local TTL coupling variations due to the offsets are displayed.

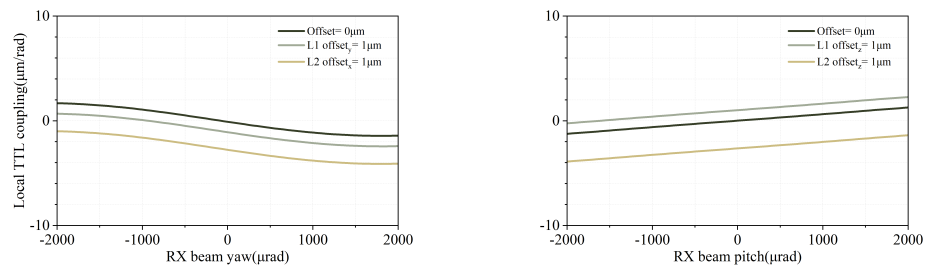


**Figure 9.** Results of the assembly errors simulation. The offset is suppressed to  $\pm 1 \mu\text{m}$ . The local TTL coupling variations due to the offsets are given.

Given the TTL coupling coefficients in the above table together with the attitude variation of a satellite, the LRI ranging error may be obtained. From the GRACE Follow-on data, the attitude variation is at the level of mrad; this generates a ranging error of approximately 20 nm. It is expected that local TTL may be, to a large extent, suppressed by careful assembly of the optical bench and choice of optical components. Further experimental work is needed to further assess the margin of errors for each source.

**Table 2.** Summary of the main sources of the local TTL coupling in yaw and pitch degrees of freedom, respectively. Estimates on the TTL coupling variation is given.

Main Sources	Degrees of Freedom	TTL Coupling Coefficients	Origin of TTL Noise
Optical components	Yaw	< 2 $\mu\text{m}/\text{rad}$ @QPD1 < 2 $\mu\text{m}/\text{rad}$ @QPD2	The imperfect imaging of the lens systems and the impact of the mismatch between the interfering beams.
	pitch	< 1.5 $\mu\text{m}/\text{rad}$ @QPD1 < 3.5 $\mu\text{m}/\text{rad}$ @QPD2	
Piston effect (lateral)	Yaw	< 3 $\mu\text{m}/\text{rad}$	Additional LPS variation due to the offset between the pivot and the reflective point of the FSM.
	pitch	< 2 $\mu\text{m}/\text{rad}$	
Piston effect (longitudinal)	Yaw	< 1 $\mu\text{m}/\text{rad}$	The longitudinal offset should be kept under 200 $\mu\text{m}$ and the lateral offset should be kept under 800nm
	pitch	< 3 $\mu\text{m}/\text{rad}$	
misalignment $L2_x$	Yaw	< 4 $\mu\text{m}/\text{rad}$	Misalignment of L2 in $x$ -axis, offset is set to be 1 $\mu\text{m}$ .
misalignment $L1_y$	Yaw	< 2.5 $\mu\text{m}/\text{rad}$	Misalignment of L1 in $y$ -axis, offset is set to be 1 $\mu\text{m}$ .
misalignment $L2_z$	pitch	< 4 $\mu\text{m}/\text{rad}$	Misalignment of L2 in $z$ -axis, offset is set to be 1 $\mu\text{m}$ .
misalignment $L1_z$	pitch	< 2.5 $\mu\text{m}/\text{rad}$	Misalignment of L1 in $z$ -axis, offset is set to be 1 $\mu\text{m}$ .

#### 4. Global TTL Coupling

Due to assembly error, thermoelasticity of the optical bench, and possibly other factors, there is an offset between the reference point and the CoM of the satellite. Apart from the planned drag-free mission by ESA in the joint NASA/ESA mission MAGIC [16], future NGGM missions will rely on the magnetic torquer for attitude control, supplemented by cold gas thrusters when a magnetic torquer is not working properly. The origins of attitude jitter come mainly from solar pressure, atmospheric drag, and albedo in the pitch direction. The attitude jitter originated from solar pressure gradient, and atmospheric drag will generate random motion of the laser link between two spacecraft. Coupled with the non-zero separation between the reference point and the CoM of the satellite, a global source of TTL is generated between two satellites which, dependent on the offset distance, does not seem to be avoidable. At the same time, the local TTL noise of the optical bench in one spacecraft will propagate with the TX beam to the distant spacecraft and couple with the random attitude jitter of the distant spacecraft. We shall study both sources of global TTL noise in this section.

Due to certain computational limitations of the IfoCAD software employed in this work [17], the relative motion between satellites is simplified as a single optical bench rotating around the RP point. A remote photodiode is placed 100km away from the TX-RP point, acting as a simplified model of the remote satellite, as depicted in Figure 10 [7,9]. The optical bench layout shown in Figure 3 is only a possible setup to reduce the offsets between the CoM and the reference point. Our main purpose is to analyze the performance of the optical bench given in Figure 1. The setup of Figure 10 is based on the layout described in Figure 1. The TX beam transmitting from the local optical bench propagates to the remote PD and interferes with a Gaussian beam placed on the surface of the remote photodiode; the beatnote is then captured by the remote photodiode. The Gaussian beam on the remote PD represents the LO beam of the remote optical bench, and the waist radius should be large enough to reduce the effect caused by the wavefront of the beams. As in the previous section, a mode expansion method is employed to study the propagation of a flat-top beam. The global TTL coupling is then obtained by combining the LPS variations derived from the local and the remote photodiodes. In addition, linear regression is employed here to estimate the margin on TTL coupling variation.

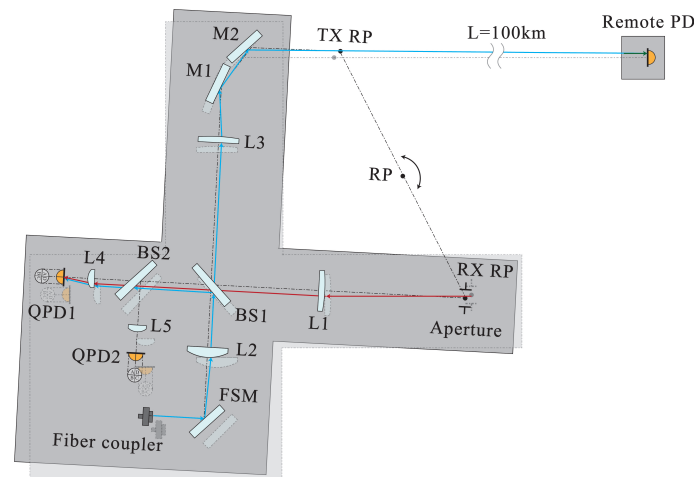


**Figure 10.** Illustration of the global TTL coupling noise. The local optical bench is rotated along the RP point in different rotational degrees of freedom. A photodiode, with a sufficient active area, represents the remote satellite located at 100km away from the TX-RP of the local optical bench [7].

#### 4.1. Reference Point Offset and Attitude Jitter

To estimate the TTL coupling noise generated by the coupling of the offset with attitude jitter, the centre of rotation of the optical bench is slightly shifted to a new point away from RP, and the optical bench is rotated around the new centre of rotation for  $\pm 2$  mrad in yaw and pitch degrees of freedom, respectively. In the case of the GRACE Follow-on mission, The offset between the vertex point of the TMA and the CoM is of the order of  $100 \mu\text{m}$  [18,19]. We shall set this as the maximum offset in our simulation. At the same time, the proposed optical design contains an open loop that can be used to control the position of RP on orbit (see Figure 3). Preliminary estimates indicate that the offset may be minimised to the level of  $\mu\text{m}$ . We shall study the TTL noise within the range of  $1 \mu\text{m}$  and  $100 \mu\text{m}$ . Results are shown in Figure 11.

Further simulation results reveal that the global TTL coupling of the pitch degree of freedom is mainly affected by the deviations on the z-axis, while the change of the global TTL coupling in the yaw degree of freedom is mainly affected by the offsets on the y-axis, depicted in Figure 11. For an offset of  $100 \mu\text{m}$  in y and z, respectively, a global TTL variation of  $200 \mu\text{m}/\text{rad}$  is generated, which must be suppressed. For the GRACE Follow-on mission, the reference point offset is approximately  $100 \text{mm}$ . However, even though this quantity is known after calibration, it can only be subtracted in the 1B data processing. In our design, it is hoped that this offset may be corrected on orbit. The reasons for doing this are as follows. Firstly, with a view that future NGGM and beyond will have better LRI measurement sensitivity to the level of a few tenths of nm, it is not clear whether the standard orbit manoeuvre is able to go under the micrometer level. Secondly, from the perspective of technological development and lessons to be learnt for gravitational wave detection, it would be instructive if we have a way to suppress the reference point offset on board. For a comparison with the GRACE Follow-on mission, given that the attitude jitter is around mrad, a TTL coupling factor of  $200 \text{mm}$  per radian will generate  $100 \text{nm}$  in LRI ranging error. This is smaller than that of the GRACE Follow-on mission, but still a subtraction in the 1B processing is needed. Offset between the RP and the CoM in the proposed new off-axis design is expected to be reduced to the level of  $1 \mu\text{m}$  by an open loop RP correction mechanism in orbit, and results are shown in Figure 12. According to the parameters used in our IfoCAD simulation, the resolution and the tilt angle of the FSM used in the open loop can be easily achieved by commercial components. Even for commercial products, the resolution can reach approximately  $20 \text{nrad}$ . For the piston noise, our experience in gravitational wave detection suggests that we may reduce it to a very low level and will not disturb the nanometer level measurement. The result of micrometer

is not a very demanding requirement for an FSM. Currently, we are also looking at an alternative optical method to adjust the reference point offset.

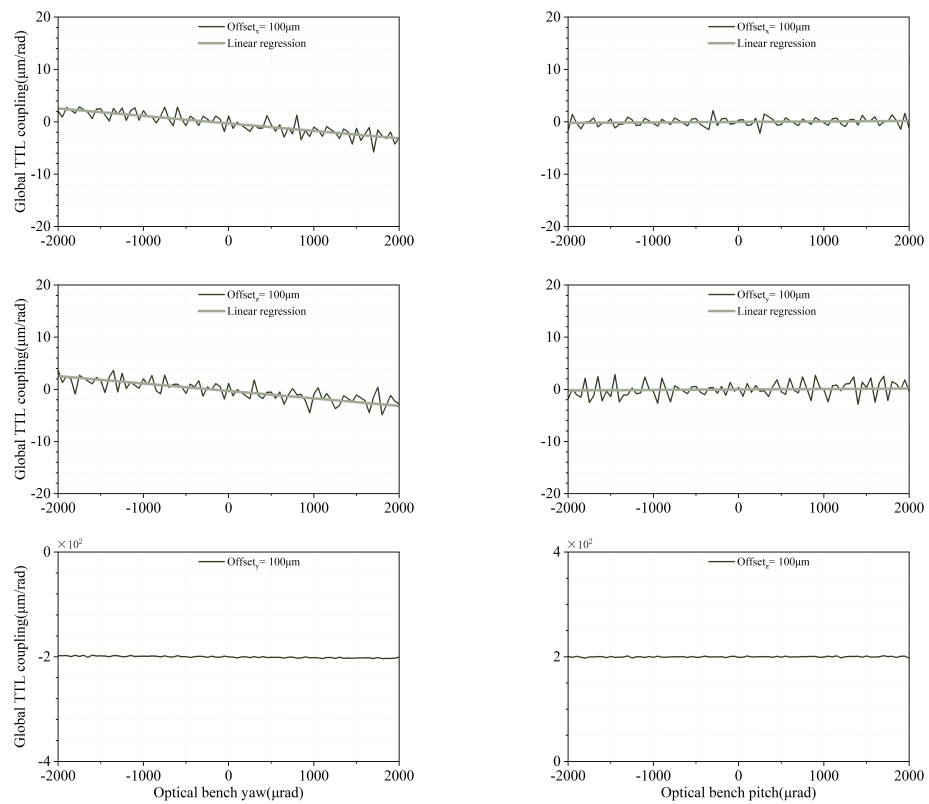


**Figure 11.** Global TTL coupling variations due to the offsets between the RP point and the CoM. The centre of rotation of the optical bench is slightly shifted to a new point away from RP in  $x$ ,  $y$ , and  $z$ , respectively, and the optical bench is rotated around the new centre of rotation for  $\pm 2$  mrad in yaw and pitch degrees of freedom, respectively. The global TTL coupling and its linear regression estimates are given.

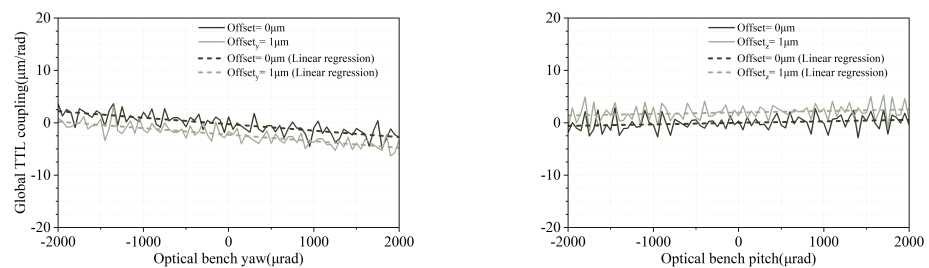


**Figure 12.** Global TTL coupling variations due to the offsets between the RP point and the CoM. Offset between the RP and the CoM is expected to be reduced to the level of  $1 \mu\text{m}$  by an open loop correction mechanism.

#### 4.2. Attitude Jitter from GRACE Follow-on 1B SCA and GNI Data

To further check on the TTL coupling coefficients calculated, we shall input the GRACE Follow-on 1B SCA and GNI data as our attitude jitter in the simulation, where SCA is the acronym of the star camera assembly and GNI is the trajectory states in the inertial frame [20]. December 2019 marked the beginning of solar cycle 25. The Sun's activity has quickly ramped up and is expected to reach a solar maximum in 2025. Among other possible effects on a satellite, the heating of the atmosphere will generate more drag on a satellite and result in worsened attitude jitter. The employment of the GRACE Follow-on 1B SCA and GNI data during this solar active period in our simulation will enable us to

understand better in a realistic way the global TTL noise in this suboptimal scenario [21]. This will help in our mission design in working out a more generous margin for attitude jitter. Data from 00:00:00.00 to 02:46:40.00 on 29 December 2022 is employed.

The attitude jitter used in the simulation is depicted in Figure 13. The local optical bench is rotated along the shifted rotation point in yaw and pitch degrees of freedom. The DWS control loop is activated and the LPS signal variation due to the attitude jitter is derived. The power spectral density of the LPS variation is then computed, as given in Figure 14.

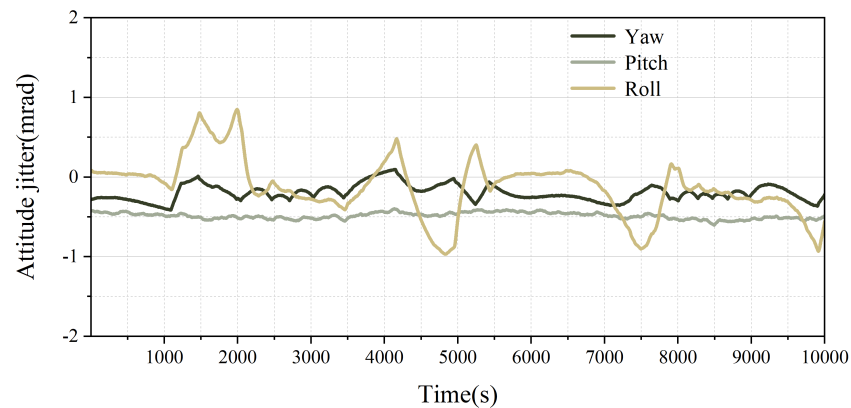


**Figure 13.** Attitude jitter in yaw, pitch, and roll degrees of freedom from the 1B SCA and GNI data of the GRACE Follow-on mission. Data of 10,000 s is taken.

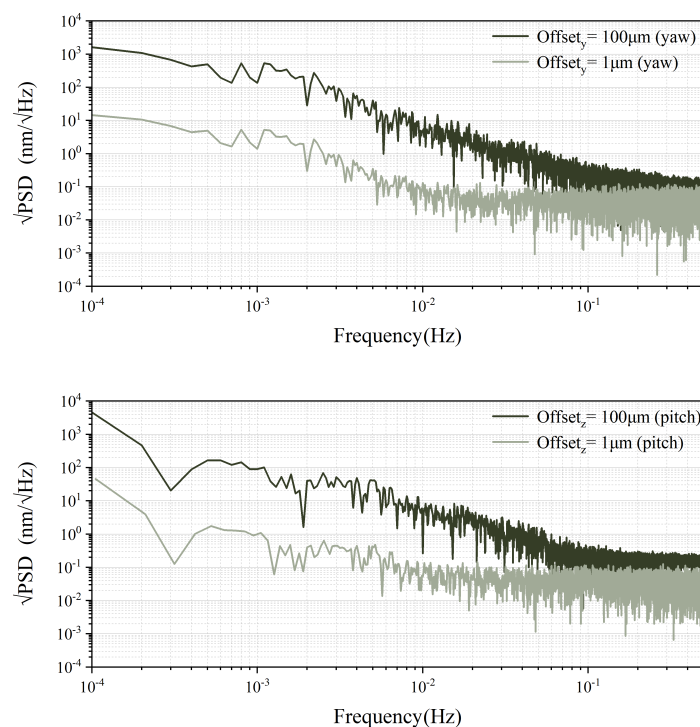


**Figure 14.** The GRACE Follow-on 1B SCA and GNI data is employed in the simulation. The power spectral density of the LPS variation in yaw and pitch are derived, with offsets of 100  $\mu\text{m}$  and 1  $\mu\text{m}$  between the RP and the CoM in  $y$  and  $z$ .

### 4.3. Cross Coupling between Local and Global TTL

Beam tilt due to local TTL coupling will generate RP point variation, and this in turn will give rise to global TTL when this couples with the relative attitude jitter between two spacecraft. We will evaluate the impact of this cross talk on the global TTL incurred.

#### 4.3.1. Global TTL Coupling and Optical Bench

The TX and LO beams of the off-axis layout originate from the same beam injected by the fibre coupler, which is then split by beamsplitter BS1. When the optical bench rotates, the optical pathlength of the TX beam passing through the BS1 changes, due to the change in the refractive index and the impact of the component wedge. The position of the TX RP then changes, resulting in an offset between the RP and the CoM.

To evaluate the global TTL generated, the local optical bench is rotated around the RP point for  $\pm 2$  mrad in yaw and pitch degrees of freedom, respectively. LPS variations derived in the local and remote photodiode are calculated. The simulation results are shown in Figure 15. The figures depict the global TTL coupling generated by the rotation of the local optical bench. The parameters utilized in the simulation are shown in Table 1.

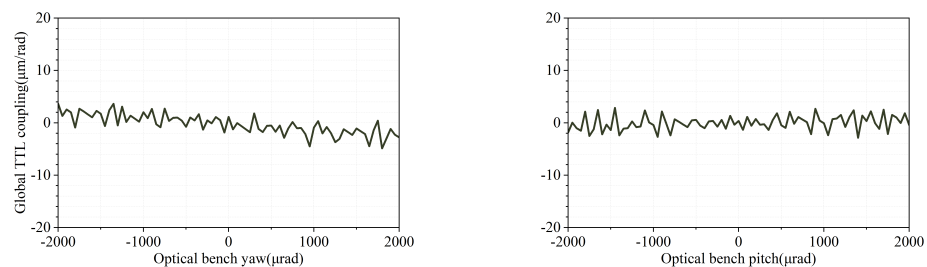


**Figure 15.** Results of the global TTL coupling simulation. The figures depict the global TTL coupling generated by the rotation of the local optical bench. The local optical bench is rotated around the RP point for  $\pm 2$  mrad in yaw and pitch degrees of freedom, respectively.

Torque exerted by non-gravitational force on a satellite will generate jitter in the roll degree of freedom. Due to assembly errors, angular misalignment is generated between the line of sight vector joining the two centres of mass of the two satellite and the laser link. In addition, the principal axes of inertia of the satellite as a rigid body deviate from the satellite body frame, and cross talk exists among different rotational degrees or freedom. These all contribute to the TTL noise in the roll degree of freedom. To estimate the global TTL coupling in roll, an angular offset between the line connecting the RPs and the laser link between satellites is introduced by rotating the local optical bench around the RP point. The optical bench is rotated around the RP point first for  $0.1 \mu\text{rad}$  in the pitch degree of freedom and then  $\pm 2$  mrad in the roll degree of freedom. LPS variations are calculated and the global TTL coupling result is obtained, as depicted in Figure 16.

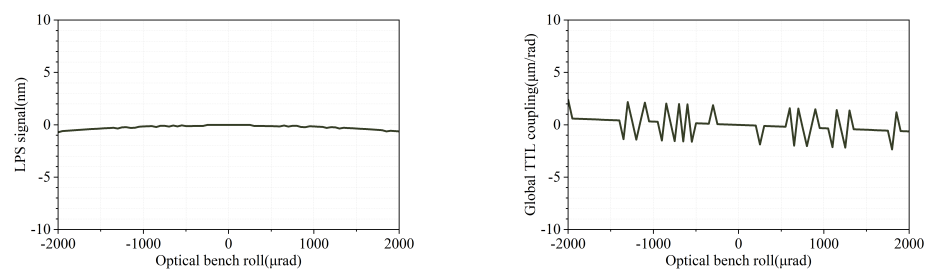


**Figure 16.** Results of the global TTL coupling simulation in roll degree of freedom. The optical bench is rotated around the RP point first for  $0.1 \mu\text{rad}$  in the pitch degree of freedom and then  $\pm 2$  mrad in the roll degree of freedom. The LPS variation and the global TTL coupling are given.

#### 4.3.2. Piston Effect

The phase variation due to the piston effect is carried by the TX beam and captured by the remote PD. For the IfoCAD simulation, the parameter of a commercial S-330 piezo actuator produced by the PI company is used to evaluate the impact caused by the piston effect. The offset between the pivot point and the reflection point of the FSM mirror is set to be 11.5 mm, and the results are given in Figure 17. The global TTL variation due to the piston effect is much smaller than that of the local situation, even with a larger longitudinal offset between the pivot of the FSM and the reflection point.

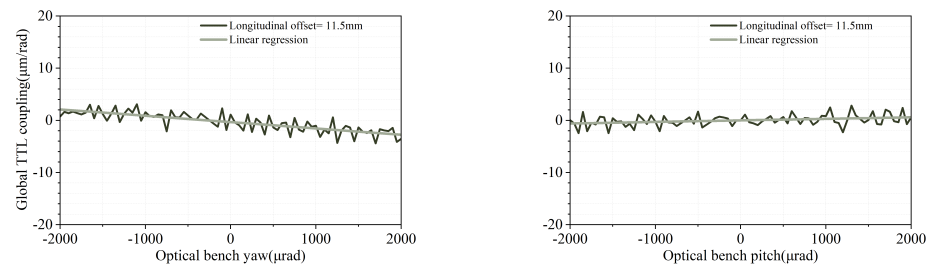


**Figure 17.** Global piston effect results. The additional offset between the pivot point and the reflection point of the FSM mirror is set to be 11.5 mm in the simulation.

#### 4.3.3. Misalignment of the Critical Components

To investigate the coupling between the global TTL coupling and the assembly errors of the local optical bench, misalignment of  $1 \mu\text{m}/\text{rad}$  for lenses L1, L2, and L3 are considered in the global TTL simulation mode, and the results are shown in Figure 18.

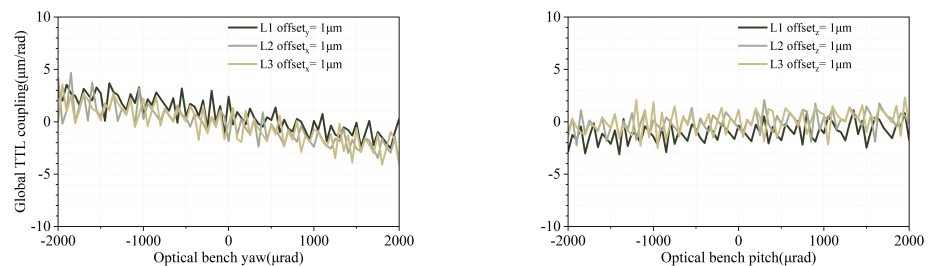


**Figure 18.** Results of the global variation due to misalignment of the critical components. Different offsets of the critical components along the three translation axes are chosen, and the positions of the components are shifted. The global TTL coupling variations due to the offsets are given.

#### 4.3.4. Misalignment of the Rooftop Mirrors

For the off-axis optical bench design, the angle between the rooftop mirrors is proposed to be  $135^\circ$ . However, an angular offset occurs due to the assembly error, resulting in an additional OPD variation. For the TMA employed in the GRACE Follow-on mission, the initial beam coalignment is required to be better than  $10 \mu\text{rad}$  [22]. The misalignment and non-orthogonality of the three mirrors in the TMA contribute to the anti-parallelism errors between the RX and the TX beams. For the rooftop mirrors, the assembly of the rooftop mirrors is easier and a higher accuracy of beam coalignment is expected to be achieved. To investigate the global TTL coupling due to the misalignment of M1 and M2, offsets of the rooftop mirrors, respectively of  $2.5 \mu\text{rad}$  and  $5 \mu\text{rad}$ , are considered in our simulation. The results are shown in Figure 19. It can be seen that an offset of  $5 \mu\text{rad}$  results in a TTL coupling variation of less than  $2.5 \mu\text{m}/\text{rad}$  in the yaw degree of freedom, and causes no significant change in the pitch degree of freedom.

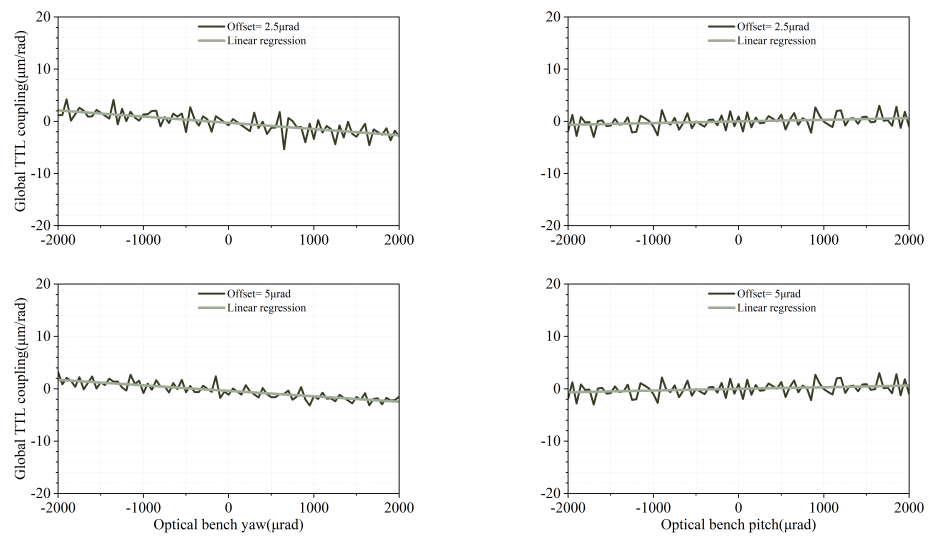


**Figure 19.** Results of the rooftop mirrors misalignment simulation. Angular offsets of the rooftop mirrors, respectively of 2.5  $\mu\text{rad}$  and 5  $\mu\text{rad}$ , are considered in the simulation.

#### 4.4. Summary of the Global TTL Coupling

To end this section, a summary is given on the cross talk between local and global TTL coupling in yaw and pitch degrees of freedom, respectively. The results are shown in Table 3. With a 2 mrad angular jitter, estimates on the margin on TTL coupling variation are given.

**Table 3.** Summary of the global TTL coupling in yaw and pitch degrees of freedom, respectively. Estimates on margin on TTL coupling variation are given.

Main Sources	Degrees of Freedom	TTL Coupling Coefficients	Origin of TTL Noise
Optical components	Yaw	<3 $\mu\text{m}/\text{rad}$	The variation of the RP point and the coupling with the residual local TTL coupling
	pitch	<1 $\mu\text{m}/\text{rad}$	
Piston effect	Yaw	<3 $\mu\text{m}/\text{rad}$	Additional LPS variation due to the offset between the pivot and the reflective point of the FSM.
	pitch	<1 $\mu\text{m}/\text{rad}$	
RP&CoM offset <sub>y</sub>	Yaw	<5 $\mu\text{m}/\text{rad}$	Misalignment between RP and CoM in $y$ -axis, offset is set to be 1 $\mu\text{m}$ .
RP&CoM offset <sub>z</sub>	pitch	<3 $\mu\text{m}/\text{rad}$	Misalignment between RP and CoM in $z$ -axis, offset is set to be 1 $\mu\text{m}$ .
misalignment L1 <sub>y</sub> misalignment L1 <sub>z</sub>	yaw	<3 $\mu\text{m}/\text{rad}$	Misalignment of L1 in $y$ -axis, offset is set to be 1 $\mu\text{m}$ . Misalignment of L1 in $z$ -axis, offset is set to be 1 $\mu\text{m}$ .
	pitch	<2 $\mu\text{m}/\text{rad}$	
M1&M2 offset	Yaw	<2.5 $\mu\text{m}/\text{rad}$	Additional TTL coupling variation due to the misalignment of the rooftop mirrors. Additional offset of 5 $\mu\text{rad}$ is introduced.
	pitch	<1 $\mu\text{m}/\text{rad}$	

Given the TTL coupling coefficients in the above table, together with the data for relative attitude variation between two satellites, the LRI ranging error may be obtained. From the GRACE Follow-on data, the attitude variation is at the level of mrad, and this generates a ranging error of approximately 20 nm. Further suppression of local TTL may reduce the noise budget of global TTL. More experimental work is needed to further assess the margin of errors for each source.

## 5. Concluding Remarks

In the present work, a new optical design alternative to that of the GRACE Follow-on mission is proposed for future NGGM missions. A detailed investigation is made on the TTL coupling noise for the new off-axis optical design. The margin of error of the TTL noise originating from different sources are carefully considered. This is in tandem with the ongoing experimental work to understand the optics and engineering aspects of the design.

With laser frequency stability designed to be  $30\text{Hz}/\sqrt{\text{Hz}}$ , laser frequency noise is approximately 10 nm. According to the calculations presented in this work, TTL is expected to be the major noise in the LRI ranging. Our analysis indicates that, given that the attitude jitter of spacecraft is at the mrad level, both local and global TTL will add up to approximately 40 nm. Though it is within the noise budget of NGGM (60–80 nm), in real experimental situations we hope to further reduce the noise to a lower level by manipulating the optical components to generate differential mode cancellation. With a good understanding on the noise sources for the optical design, a solid foundation is hopefully laid for further experimental work and optimisation of the optical design. The present work only serves as a guide to our tabletop prototype development.

**Author Contributions:** Conceptualization, J.W. and Y.Y.; methodology, K.W., J.W., B.P., Y.Y. and Y.-K.L.; software, K.W. and B.P.; formal analysis, K.W. and J.W.; investigation, K.W., J.W. and B.P.; resources, J.J., Y.W., Y.Z., Y.Y., X.L. and Y.-K.L.; data curation, K.W.; writing—original draft preparation, K.W., J.W., B.P. and Y.-K.L.; writing—review and editing, Y.-K.L.; supervision, H.L., X.L. and Y.-K.L.; project administration, X.L. and Y.-K.L.; funding acquisition, Y.-K.L. All authors have read and agreed to the published version of the manuscript.

**Funding:** The present work is supported by the National Key Research and Development Program of China under grant number 2021YFC2202501 and NSFC grant number 12247101.

**Acknowledgments:** We benefit immensely from many discussions with our AEI colleagues, and Vitali Müller in particular. The optical design was worked out by Yichao Yang while he was visiting AEI through the LEGACY program of the MPG-CAS collaboration scheme in gravitational physics.

**Conflicts of Interest:** The authors declare no conflict of interest.

## References

1. Abich, K.; Abramovici, A.; Amparan, B.; Baatzsch, A.; Okihiro, B.B.; Barr, D.C.; Bize, M.P.; Bogan, C.; Braxmaier, C.; Burke, M.J.; et al. In-Orbit Performance of the GRACE Follow-on Laser Ranging Interferometer. *Phys. Rev. Lett.* **2019**, *123*, 031101. [[CrossRef](#)] [[PubMed](#)]
2. Massotti, L.; Siemes, C.; March, G.; Haagmans, R.; Silvestrin, P. Next Generation Gravity Mission Elements of the Mass Change and Geoscience International Constellation: From Orbit Selection to Instrument and Mission Design. *Remote Sens.* **2021**, *13*, 3935. [[CrossRef](#)]
3. Xiao, Y.; Yang, Y.; Pan, Z.; Liu, X.; Sun, Z. Performance and application of the Chinese satellite-to-satellite tracking gravimetry system. *Chin. Sci. Bull.* **2023**, *68*, 2655–2664. (In Chinese). [[CrossRef](#)]
4. Kornfeld, R.P.; Arnold, B.W.; Gross, M.A.; Dahya, N.T.; Klipstein, W.M.; Gath, P.F.; Bettadpur, S. GRACE-FO: The Gravity Recovery and Climate Experiment Follow-On Mission. *J. Spacecr. Rocket.* **2019**, *56*, 931–951. [[CrossRef](#)]
5. Mandel, O.; Sell, A.; Chwalla, M.; Schuldt, T.; Krauser, J.; Weise, D.; Braxmaier, C. Architecture and performance analysis of an optical metrology terminal for satellite-to-satellite laser ranging. *Appl. Opt.* **2020**, *59*, 653–661. [[CrossRef](#)] [[PubMed](#)]
6. Pfaffenzeller, N.; Pail, R. Small satellite formations and constellations for observing sub-daily mass changes in the Earth system. *Geophys. J. Int.* **2023**, *234*, 1550–1567. [[CrossRef](#)]
7. Wu, K.; Peng, B.; Lin, X.; Luo, H.; Wang, Y.; Wu, J.; Shen, X.; Chang, X.; Lau, Y.K.; Zheng, Y.; et al. Off-axis Optical Bench Design for Next Generation Gravity Mission. In Proceedings of the International Conference on Space Optics (ICSO), Dubrovnik, Croatia, 3–7 October 2022.
8. Müller, V. Design Considerations for Future Geodesy Missions and for Space Laser Interferometry. Ph.D. Thesis, Gottfried Wilhelm Leibniz Universität Hannover, Hannover, Germany, 2017.
9. Yang, Y.; Yamamoto, K.; Dovale Álvarez, M.; Wei, D.; Esteban Delgado, J.J.; Müller, V.; Jia, J.; Heinzl, G. On-Axis Optical Bench for Laser Ranging Instruments in Future Gravity Missions. *Sensors* **2022**, *22*, 2070. [[CrossRef](#)] [[PubMed](#)]
10. Dehne, M. Construction and Noise Behaviour of Ultra-Stable Optical Systems for Space Interferometers. Ph.D. Thesis, University of Hannover, Hannover, Germany, 2012.
11. Mahrdt, C. Laser Link Acquisition for the GRACE Follow-On Laser Ranging Interferometer. Ph.D. Thesis, Gottfried Wilhelm Leibniz Universität Hannover, Hannover, Germany, 2014.

12. Schilling, R. Available online: <http://www2.mpg.de/~ros/optocad/> (accessed on 30 January 2022).
13. Furun, W. Study on Center of Mass Calibration and K-Band Ranging System Calibration of the GRACE Mission. Ph.D. Thesis, The University of Texas at Austin, Austin, TX, USA, 2003.
14. Hartig, M.S.; Schuster, S.; Wanner, G. Geometric tilt-to-length coupling in precision interferometry: Mechanisms and analytical descriptions. *J. Opt.* **2022**, *24*, 065601. [[CrossRef](#)]
15. Witvoet, G.; Human, J.; Maniscalco, M. Realization and testing of an active mirror mechanism for in-field pointing in eLISA. In *Advances in Optical and Mechanical Technologies for Telescopes and Instrumentation II*; SPIE: Bellingham, WA, USA, 2016; Volume 9912, pp. 1901–1908.
16. Cesare, S.; Dionisio, S.; Saponara, M.; Bravo-Berguño, D.; Massotti, L.; Teixeira da Encarnação, J.; Christophe, B. Drag and Attitude Control for the Next Generation Gravity Mission. *Remote Sens.* **2022**, *14*, 2916. [[CrossRef](#)]
17. IfoCAD. Available online: <https://www.aei.mpg.de/ifocad> (accessed on 12 June 2023).
18. Müller, V.; Hauk, M.; Misfeldt, M.; Müller, L.; Wegener, H.; Yan, Y.; Heinzl, G. Comparing GRACE-FO KBR and LRI Ranging Data with Focus on Carrier Frequency Variations. *Remote Sens.* **2022**, *14*, 4335. [[CrossRef](#)]
19. Henry, W. Analysis of Tilt-To-Length Coupling in the GRACE Follow-on Laser Ranging Interferometer. Ph.D. Thesis, Gottfried Wilhelm Leibniz Universität, Hannover, Germany, 2022.
20. JPL. *Gravity Recovery and Climate Experiment Follow-on (GRACE-FO) Level-1 Data Product User Handbook*; JPL D-56935 (URS270772); JPL: Pasadena, CA, USA, 2019.
21. GFO Data. Available online: <https://podaac-tools.jpl.nasa.gov/drive/files/allData/gracefo/L1> (accessed on 25 January 2023).
22. Daniel, S. Intersatellite Laser Interferometry: Test Environments for GRACE Follow-on. Ph.D. Thesis, Leibniz University Hannover, Hannover, Germany, 2014.

**Disclaimer/Publisher’s Note:** The statements, opinions and data contained in all publications are solely those of the individual author(s) and contributor(s) and not of MDPI and/or the editor(s). MDPI and/or the editor(s) disclaim responsibility for any injury to people or property resulting from any ideas, methods, instructions or products referred to in the content.